Stationary crack tip fields in elastic–plastic solids: an overview of recent numerical simulations

2009 J. Phys. D: Appl. Phys. 42 214005

(http://iopscience.iop.org/0022-3727/42/21/214005)

IOP PUBLISHING JOURNAL OF PHYSICS D: APPLIED PHYSICS

J. Phys. D: Appl. Phys. **42** (2009) 214005 (15pp) doi:10.1088/0022-3727/42/21/214005

Stationary crack tip fields in elastic–plastic solids: an overview of recent numerical simulations

R Narasimhan[1], H Y Subramanya[2], S D Patil[1], Parag Tandaiya[1] and U Ramamurty[3]

[1] Department of Mechanical Engineering, Indian Institute of Science, Bangalore, 560 012, India
[2] Structural Technologies Division, National Aerospace Laboratories, Bangalore 560017, India
[3] Department of Materials Engineering, Indian Institute of Science, Bangalore 560 012, India

E-mail: narasi@mecheng.iisc.ernet.in

Received 24 December 2008, in final form 4 March 2009
Published 22 October 2009
Online at stacks.iop.org/JPhysD/42/214005

Abstract

In this paper, an overview of some recent numerical simulations of stationary crack tip fields in elastic–plastic solids is presented. First, asymptotic analyses carried out within the framework of 2D plane strain or plane stress conditions in both pressure insensitive and pressure sensitive plastic solids are reviewed. This is followed by discussion of salient results obtained from recent computational studies. These pertain to 3D characteristics of elastic–plastic near-front fields under mixed mode loading, mechanics of fracture and simulation of near-tip shear banding process of amorphous alloys and influence of crack tip constraint on the structure of near-tip fields in ductile single crystals. These results serve to illustrate several important features associated with stress and strain distributions near the crack tip and provide the foundation for understanding the operative failure mechanisms. The paper concludes by highlighting some of the future prospects for this field of study.

(Some figures in this article are in colour only in the electronic version)

1. Introduction

Modern design of structures and their components is becoming increasingly complex, primarily for the following two reasons. First, newer and more advanced materials (e.g. metallic glasses, shape memory alloys, etc), whose constitutive behaviour is significantly different from that of conventional engineering materials, are being developed. Secondly, there is an increasing demand from users for an accurate assessment of the structural integrity and reliability as well as implementation of these requirements in design. The goal is to design optimal structures and at the same time ensure that they are fail-safe under all possible service conditions. In this context, fracture mechanics assumes an important role, as it enables one to assess and understand a material's response in the presence of flaws, which limit its strength and life, under a variety of loading conditions. In addition, it allows for identification of suitable fracture characterizing parameters such as the stress intensity factor, K, or the energy release rate J.

An important aspect in fracture mechanics is the examination of crack tip fields. The concept of 'similitude', which implies that the intensity of the crack tip fields in any given structure is uniquely determined by the applied value of K or J, as appropriate, is central to the theory of fracture mechanics. It is important to critically understand the near-tip stress and strain distributions for a variety of different materials. This is not only useful in structural design but also helps in understanding material failure by shedding light on potential fracture mechanisms (e.g. brittle cleavage or ductile void coalescence). This allows one to identify the origin (or the lack thereof) of a material's toughness from a continuum standpoint and, in turn, develop fracture resistant advanced materials. Further, crack tip fields in combination with a local fracture initiation criterion can also help in predicting

the potential direction of crack propagation especially under mixed mode loading conditions thereby enabling the designer to take corrective measures.

A considerable amount of research work has been carried out using analytical and numerical techniques to investigate crack tip fields in inelastic materials since they were first studied by Hutchinson [1, 2] and Rice and Rosengren [3]. Given this background, some salient results from recent simulations of stationary crack tip fields in elastic–plastic materials are reviewed in this paper. Since a comprehensive review of all the developments is not possible within the limited space available, some selected results are presented to illustrate the recent advances, especially pertaining to non-traditional materials such as amorphous alloys and ductile single crystals. First, asymptotic studies carried out within the framework of 2D plane strain or plane stress conditions in both pressure insensitive and pressure sensitive plastic solids are reviewed in section 2. This is followed by discussion of some recent results on 3D effects near the crack front under mixed mode (combined modes I and II) loading in section 3. In section 4, stress and strain distributions near the crack tip in amorphous alloys, as well as formation of multiple shear bands inside the plastic zone, are studied through finite element simulations. These simulations employ a recently proposed sophisticated constitutive model for metallic glasses. It must be noted that amorphous alloys display an intriguing mechanical behaviour, but nevertheless possess attractive properties, and hence, have many potential engineering applications ranging from biomedical to sporting equipment. Finally, in section 5, recent finite element simulations that highlight the role played by crack tip constraint in altering the stress and plastic slip distributions near the tip (in particular, formation of slip shear bands and kink shear bands) in ductile single crystals are described. The results from these simulations corroborate well with recent experimental observations on aluminium single crystal specimens having low and high constraint. They are important, both due to some high technological applications of single crystals and also due to the fact that when the length scale influenced by the crack tip shrinks, the fields are essentially embedded within a single grain so that local slip activity dominates crack tip plasticity.

Thus, the results discussed in this paper serve to illustrate several important features associated with stress and strain distributions near the crack tip in elastic–plastic solids and provide the foundation for understanding the operative failure mechanisms. The paper concludes by highlighting some of the future prospects for this field of study.

2. Asymptotic studies on stationary crack tip fields

2.1. Pressure insensitive plastic solids

In this section, asymptotic studies on stress and strain fields near stationary crack tips in pressure insensitive elastic–plastic solids are reviewed. All these studies have been carried out under the conditions of 2D plane strain or plane stress. Hutchinson [1, 2] and Rice and Rosengren [3] analysed the dominant singular fields near a stationary crack tip in power law hardening plastic solids under mode I loading. Their asymptotic solution, which is commonly referred to as the HRR solution, revealed several important features about the structure of the stress and strain variations near the crack tip and paved the way for the development of the field of elastic–plastic fracture mechanics. In their work, they assumed that the uniaxial stress–strain curve is described by a Ramberg–Osgood relation, which is given by

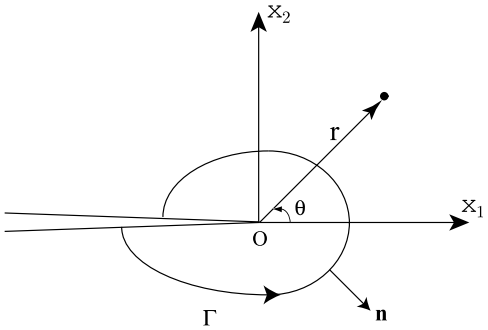

Figure 1. Schematic showing the conventions for the coordinate system and an arbitrary contour Γ surrounding the crack tip.

$$\frac{\epsilon}{\epsilon_o} = \frac{\sigma}{\sigma_o} + \alpha \left(\frac{\sigma}{\sigma_o}\right)^n, \tag{1}$$

where σ_o is the initial yield stress, $\epsilon_o = \sigma_o/E$ is the initial yield strain and α, n are material parameters. It must be noted that higher values of hardening exponent n imply less strain hardening. As the crack tip is approached, the first term in the right hand side of (1) can be neglected in comparison with the second term. The small strain, J_2 deformation theory of plasticity, which is like a nonlinear elasticity model, is used to generalize (1) to multi-axial states.

In [1, 3], a separable form in polar coordinates (r, θ) centred at the crack tip (see figure 1) was assumed as $r^s f(\theta)$ for the dominant term in the strain variation. A straightforward analysis based on the path independence of the J-integral shows that $s = -n/(n+1)$. Here, it must be noted that J-integral is defined by [4]

$$J = \int_\Gamma \left(W n_1 - \sigma_{ij} n_j \frac{\partial u_i}{\partial x_1} \right) \mathrm{d}s, \tag{2}$$

where $W(\epsilon)$ is the strain energy density of the material, Γ is any open contour encircling the crack tip in the counterclockwise direction and $\boldsymbol{n}$ is the unit outward normal to Γ (see figure 1). By substituting the assumed form for the asymptotic fields in the compatibility equation, a fourth-order nonlinear ordinary differential equation is obtained for the angular variation of the Airy's stress function. This equation, subjected to traction-free conditions on the crack flank ($\theta = \pi$) and mode I symmetry conditions on the line ahead of the tip ($\theta = 0$), was solved numerically using a Runge–Kutta method in [1, 3]. An alternate finite element procedure to derive the angular functions associated with the dominant singular term has been discussed by Symington *et al* [5].

The HRR fields may be expressed as [6]

$$\sigma_{ij} = \sigma_o \left(\frac{J}{\alpha \sigma_o \epsilon_o I_n r} \right)^{1/(n+1)} \tilde{\sigma}_{ij}(\theta, n), \tag{3}$$

$$\epsilon_{ij} = \alpha \epsilon_o \left(\frac{J}{\alpha \sigma_o \epsilon_o I_n r} \right)^{n/(n+1)} \tilde{\epsilon}_{ij}(\theta, n), \tag{4}$$

$$u_i - \hat{u}_i = \alpha \epsilon_o r \left(\frac{J}{\alpha \sigma_o \epsilon_o I_n r} \right)^{n/(n+1)} \tilde{u}_i(\theta, n), \tag{5}$$

where the dimensionless angular functions $\tilde{\sigma}_{ij}$, $\tilde{\epsilon}_{ij}$ and $\tilde{u}_i$ as well as the constant I_n depend on the hardening exponent n and whether plane strain or plane stress conditions prevail inside the plastic zone. The constants $\hat{u}_i$ account for a possible translation of the crack tip itself. The above dimensionless angular functions (normalized such that the angular part of the Mises equivalent stress $\tilde{\sigma}_e$ has a maximum value of unity) and the constant I_n are given in [1] for different values of n. It is important to note that the normalized opening stress $\tilde{\sigma}_{22}$ and the hydrostatic stress $\tilde{\sigma}_h = \tilde{\sigma}_{kk}/3$ are highly elevated ahead of the crack tip ($\theta = 0$), while the plastic shear strain component $\tilde{\epsilon}_{r\theta}$ is large above (or below) the crack tip under Mode I, plane strain. By contrast, under Mode I, plane stress, the stress state ahead of the tip is biaxial with the tangential plastic strain $\tilde{\epsilon}_{\theta\theta}$ attaining a large value in this region. Further, it should be observed from (3)–(5) that the J-integral, which depends on the applied load, crack length and other geometrical dimensions serves as a measure of the strength of the crack tip stress and deformation fields. However, as pointed out by Hutchinson [6], in order to use J as a valid fracture characterizing parameter, it is essential that the region of dominance of the HRR field (3), (4) should exceed the size of the fracture process zone where microscopic processes such as void growth and coalescence occur. These processes are governed by finite strains and non-proportional loading which are not represented by the small strain deformation theory of plasticity on which the HRR analysis is based. The above requirement is referred to as the condition of J-dominance [6].

Shih [7] and Hutchinson and Shih [8] extended the above solution to include combined modes I and II loading under conditions of plane strain and plane stress, respectively. Their analysis shows that while the form of the near-tip fields remains the same as (3)–(5), the normalized angular functions and I_n depend additionally on the near-tip plastic mode mixity parameter M_p defined by

$$M_p = \frac{2}{\pi} \lim_{r \to 0} \left\{ \tan^{-1} \left[\frac{\sigma_{\theta\theta}(r, \theta = 0)}{\sigma_{r\theta}(r, \theta = 0)} \right] \right\}. \tag{6}$$

Thus, M_p is a measure of the relative strengths of the normal and shear tractions on the line immediately ahead of the crack tip and is equal to 1 for pure mode I and 0 for pure mode II. Further, the results of Shih [7, 8] imply that under mixed mode loading the near-tip fields are scaled by J and parametrized by M_p. By using a special finite element procedure which embeds the singular fields (4) in the near-tip region, Shih [7] and Hutchinson and Shih [8] established under small scale yielding (SSY) conditions the relationship between M_p and the remote elastic mixity M_e defined by

$$M_e = \frac{2}{\pi} \tan^{-1} \left[\frac{K_I}{K_{II}} \right], \tag{7}$$

where K_I and K_{II} are the far-field mode I and II stress intensity factors. In subsequent studies, Pan and Shih [9–11] derived the near-tip fields for combined modes I–III, II–III and I–II–III loadings. However, it must be noted that under these conditions the singularity orders may differ from those given by the HRR solution (see [9–11]).

In many advanced materials such as ceramic and metal matrix composites and thin films deposited on substrates, interfacial fracture is a common failure mode and may limit their overall strength and ductility. In a series of investigations, Shih and Asaro [12–14] examined the stress and plastic strain distributions near a stationary crack tip that lies at the interface between two elastic–plastic materials and showed that the crack tip fields are members of a family parametrized by a plastic mode mixity parameter ξ and are scaled by J. For SSY conditions, ξ can be viewed as the overall phase angle of the plastic zone [14]. While the structure of the interfacial crack tip fields for opening-dominated loading strongly resembles the mixed mode HRR solution [7, 8] of homogeneous solids, crack tip blunting and zone of substantial plasticity are larger in the former. The above studies [12–14] also show that no crack face contact occurs over physically relevant length scales, which mitigates a pathological feature of the linear elastic solution [15]. A detailed review of elasticity and plasticity aspects associated with interfacial cracks may be found in [15].

It has been observed from numerical studies [16, 17] and fully plastic slipline solutions [18] that while the level of stress triaxiality (or crack tip constraint) under mode I, plane strain is high in geometries involving predominantly bending over the uncracked ligament, it could be lower when subjected to tensile loads. This has led to several analytical studies [19, 20] aimed at determining the higher order terms in the asymptotic solution for the crack tip fields. These were complemented by numerical investigations [21, 22] wherein two-parameter descriptions of the near-tip stress and strain variations were explored. While the two parameters were taken as the J-integral and the T-stress (the second term in the linear elastic crack tip field) by Betegon and Hancock [21], an alternative J–Q characterization of the elastic–plastic crack tip fields where Q is a triaxiality parameter was proposed by O'Dowd and Shih [22]. The latter form, which is more robust since it can be applied to both small and large scale yielding conditions, can be expressed in the forward sector ($|\theta| < \pi/2$) as [22]

$$\sigma_{ij} = (\sigma_{ij})_{HRR} + Q\sigma_o \delta_{ij}, \tag{8}$$

where the first term is the HRR field. The parameter Q is negative for low constraint fracture geometries such as center cracked panel (CCP) under tension [22]. The form (8) is consistent with a four-term asymptotic expansion obtained by Xia *et al* [20]. Roy and Narasimhan [23] found from modified boundary layer simulations that under mixed mode loading with a given remote elastic mode mixity M_e, the imposition of

a non-zero T-stress changes M_p from its value corresponding to pure SSY (i.e. $T = 0$; see [7]). This alters the stress triaxiality near the crack tip. Basu and Narasimhan [24] and Jayadevan *et al* [25] demonstrated that a valid J–Q field exists under mode I dynamic loading irrespective of the specimen geometry and loading rate. They noted that a specimen which maintains high constraint under quasi-static loading may exhibit progressive loss of triaxiality as the loading rate increases. Biswas and Narasimhan [26] showed that this inertia-driven constraint loss may be responsible for the experimentally observed enhancement in dynamic fracture toughness of ductile materials.

All the studies referenced above pertain to isotropic, pressure insensitive plastic solids obeying the von Mises yield condition. However, polycrystalline alloys may show pronounced plastic anisotropy due to preferred crystallographic orientation of the grains (or texture) arising from mechanical processing (like rolling or extrusion). Also, ductile single crystals are inherently anisotropic due to plastic flow caused by slip on distinct slip systems. Analysis of crack tip fields in ductile single crystals is discussed in section 5. Pan and Shih [27, 28] considered power law hardening orthotropic materials obeying Hill's quadratic yield function [29] under conditions of plane strain and plane stress, respectively. On choosing the coordinate axes to coincide with the principal axes of plastic orthotropy, the above yield function under plane strain (in the x_1–x_2 plane, see figure 1) reduces to:

$$\tau_e^2 = \tfrac{1}{4} p(\sigma_{11} - \sigma_{22})^2 + \sigma_{12}^2. \tag{9}$$

Here, p is a plastic anisotropy parameter (with $p = 1$ representing the isotropic or von Mises case) and τ_e is the shear yield strength with respect to the x_1–x_2 axes. A power law hardening form similar to (1) was assumed by Pan and Shih [27, 28] for the relationship between the shear strain and shear stress with respect to the above axes. The dominant crack tip fields have the same structure as (3)–(5) with additional dependence of the angular functions and the constant I_n on p. An important observation made in [27] was that for highly orthotropic materials ($p \ll 1$ or $p \gg 1$) the near-tip plastic strain field may consist of narrow bands of intense shear along certain directions.

Several experimental studies, involving micro-indentation [30], micro-torsion [31] and micro-bending [32], have indicated that plastic flow of micron-sized metal samples exhibits a strong size effect. In particular, additional strengthening occurs due to non-uniform plastic deformation on size scales of the order of a few microns owing to generation of geometrically necessary dislocations. In order to explain the observed size effect, several phenomenological plasticity theories have been proposed, all of which incorporate a dependence on strain gradient (see, for example [33–35]). From the fracture viewpoint, the effect of strain gradients is crucial in understanding how the stresses near a sharp crack tip can attain levels necessary to cause cleavage or atomic decohesion [36]. Xia and Hutchinson [37] and Huang *et al* [38] analysed stationary crack tip fields under plane strain conditions using the couple stress theory [33]. They found that the dominant displacement field is irrotational, and the normal stress ahead of the tip under mode I is about the same as that in classical plasticity [1–3]. This is attributed to the fact that the couple stress theory incorporates only rotation gradients and not stretch gradients. Jiang *et al* [39] conducted finite element analysis of a stationary crack under mode I, SSY conditions using the mechanism-based strain gradient (MSG) plasticity theory [35]. They found that the stress singularity and levels of effective and opening stresses ahead of the tip are higher than those given by the HRR solution at distances from the tip less that $0.3l$, where l is a length scale in the constitutive model. This length scale is estimated to be about 4 μm for copper [39]. Thus, the elevation in stress as predicted by the MSG theory as compared with the HRR solution occurs at distances from the tip less than about 1 μm which is still large compared with the average spacing between dislocations. However, further multi-scale modelling using discrete dislocation theory, nonlocal plasticity and conventional plasticity theories is required to understand the nature of the fields at different length scales from the crack tip.

2.2. *Pressure sensitive plastic solids*

Many engineering materials such as polymers, ceramics and metallic glasses as well as geomaterials such as rocks and soils exhibit pressure sensitive plastic behaviour [40–44]. The Drucker–Prager yield function, which is given by

$$\phi(\sigma_{ij}, \sigma_c) = \sigma_e + \sigma_h \tan\beta - \left(1 - \frac{\tan\beta}{3}\right)\sigma_c, \tag{10}$$

is commonly used to represent the plastic response of some of these materials. Here, σ_e and σ_h are the Mises equivalent stress and hydrostatic stress, respectively. Further β is a pressure sensitivity index and σ_c is the yield stress under uniaxial compression. It must be noted that the case $\beta = 0$ corresponds to the von Mises model. Li and Pan [45, 46] studied the mode I, asymptotic stationary crack tip fields in pressure sensitive, dilatant materials obeying a yield condition of the form given by (10) along with power law hardening under plane strain and plane stress conditions, respectively. They found that HRR-type solution exists (for $\kappa = \tan\beta/\sqrt{3}$ within a limiting value) with the singularity order of the stress and strain fields remaining the same as in (3) and (4). However, the angular functions and the constant I_n also depend on κ. Their results show that the stress state ahead of the crack tip relaxes with increase in κ, while the plastic strain (especially, the tangential component $\epsilon_{\theta\theta}$) enhances. This has important implications for fracture mechanisms such as craze formation or void growth in amorphous polymers [47] and shear banding in amorphous alloys (see section 4).

Yuan and Lin [48] extended the work of Li and Pan [45, 46] by deriving a two-term asymptotic expansion of the plane stress and plane strain crack tip fields. They also conducted finite element computations using a modified boundary layer formulation and confirmed that the inclusion of second order terms under plane strain conditions increases the dominance of the analytical solution considerably. It is found that an associated flow rule may tend to overestimate the extent of plastic dilatancy (see, for example, Chiang and Chai [49] for

amorphous polymers), which has motivated the use of a non-associated flow rule. Thus, the plastic part of the strain rate $\dot{\epsilon}_{ij}^{\mathrm{p}}$ is taken to be directed along the normal to a flow potential surface G, which is given by

$$G(\sigma_{ij}) = \sigma_{\mathrm{e}} + \sigma_{\mathrm{h}} \tan \psi. \tag{11}$$

On comparing (10) and (11), it may be seen that $\beta = \psi$ leads to an associated flow rule. Papanastasiou and Durban [50] noted that the use of a non-associated flow rule (with $\psi < \beta$) can slightly enhance the singularity order of the asymptotic fields (over that given by the HRR solution) in pressure sensitive plastic solids. Moreover, the plastic shear strain $\epsilon_{r\theta}$ enhances significantly when $\psi < \beta$ for large values of strain hardening exponent n. Interestingly, Rudnicki and Rice [44] have noted that shear band type instabilities which result in localized plastic deformation occur more easily in pressure sensitive plastic solids when $\psi < \beta$.

In the following sections, recent numerical studies undertaken to investigate issues such as 3D effects under mixed mode loading, crack tip fields in amorphous alloys and role of constraint in ductile single crystals are described.

3. 3D mixed mode (I and II) fields in elastic–plastic solids

The stress and deformation fields near a crack front are inherently 3D in nature. However, no analytical, asymptotic solution near a 3D crack front in an elastic–plastic solid is available in order to judge the validity of the crack tip fields reviewed in the previous section which are based on the assumptions of 2D plane strain or plane stress. Hence, detailed 3D finite element analyses are essential to characterize the stress and strain variations near a crack front in elastic–plastic solids and also ascertain the range of dominance of 2D plane strain and plane stress solutions. To this end, Nakamura and Parks [51] performed a 3D boundary layer analysis of a thin ductile plate under mode I loading. Also, Narasimhan and Rosakis [52] and Zehnder and Rosakis [53] carried out numerical (both 2D and 3D) and experimental investigations on a ductile three-point bend specimen and found strong thickness variations of stress fields and the local energy release rate J very near the crack front. Their results, and those reported by Nakamura and Parks [51], revealed that strong 3D effects are present within a radial distance of about one-half of the plate thickness from the crack front. However, the above studies were restricted to mode I loading in materials obeying the von Mises yield condition. In order to characterize the effects of pressure sensitivity and plastic dilatancy on near-front fields under mode I, Subramanya *et al* [54] conducted 3D numerical simulations using a boundary layer model similar to [51]. In their simulations, a linear Drucker–Prager yield theory(governed by (10), (11)) was employed to describe the constitutive response of the material. They observed that while pressure sensitivity leads to a significant drop in the hydrostatic stress all along the crack front, it enhances the plastic strain and crack opening displacements.

Subramanya *et al* [55] carried out extensive elastic–plastic simulations using a boundary layer (SSY) formulation

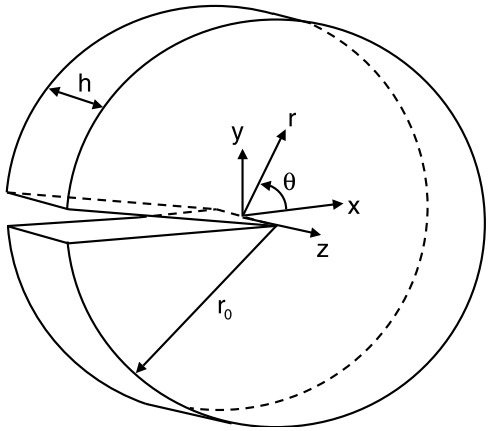

Figure 2. Schematic 3D view of a cracked circular plate of thickness h and radius r_{o} along with the coordinate system used in the boundary layer formulation of [54, 55] (reproduced with permission [85] from [55]).

to investigate the 3D nature of the near-front fields under mixed mode (combined modes I and II) loading. They considered a large circular disc (see figure 2) containing a crack lying on one of its radial planes with the straight crack front along the axis of the disc (z-axis). The mid-plane of the disc is given by $z = 0$, while $z/h = \pm 0.5$ correspond to the free surfaces of the disc. Due to symmetry, only one-half of the thickness of the disc ($z \geqslant 0$) was modelled with appropriate symmetry conditions imposed on its mid-plane. The material was taken to obey the J_2 incremental theory of plasticity with isotropic power law hardening. The values of initial yield strain σ_{o}/E and strain hardening exponent n were chosen as 0.002 and 10. The mixed mode elastic (K_{I}-K_{II}) field was prescribed as remote boundary conditions on the outer boundary of the circular disc and different values of elastic mode mixity M_{e} (see (7)) were considered. Since the size of the plastic zone relative to the disc thickness, h, has a direct bearing on the nature of the near-front fields [51], the analyses were carried out for load levels corresponding to $R_{\mathrm{p}}^{\max}/h$ values ranging from 0.1 to 5 (where, $R_{\mathrm{p}}^{\max}$ is the maximum in-plane radius of the plastic zone with respect to all z/h). Some of the salient results obtained from these simulations are discussed below.

In figures 3(a) and (b), 3D views of the plastic zone at two load levels corresponding to $R_{\mathrm{p}}^{\max}/h = 0.1$ and 0.5 are presented for the mixed mode case with $M_{\mathrm{e}} = 0.7$. In this figure, the size scale is set by the disc thickness h. The trace of the plastic zone on the free surface of the disc is highlighted by the red contour. At small load (figure 3(a)), the shape of the plastic zone all along the crack front is similar to the plane strain case (see [7]) except in a small region near the free surface. In this region ($0.4 \leqslant z/h \leqslant 0.45$), change in shape of the 3D plastic zone from plane strain [7] to plane stress case [8] has initiated at a very small load level. It must be noted that this transition to the plane stress plastic zone shape does not commence at the free surface owing to steep thickness gradient in stresses near the crack front (see figure 5) and a significant drop in the local energy release rate [51] close to the free surface. Due to these reasons, plane stress conditions are not attained at the free surface

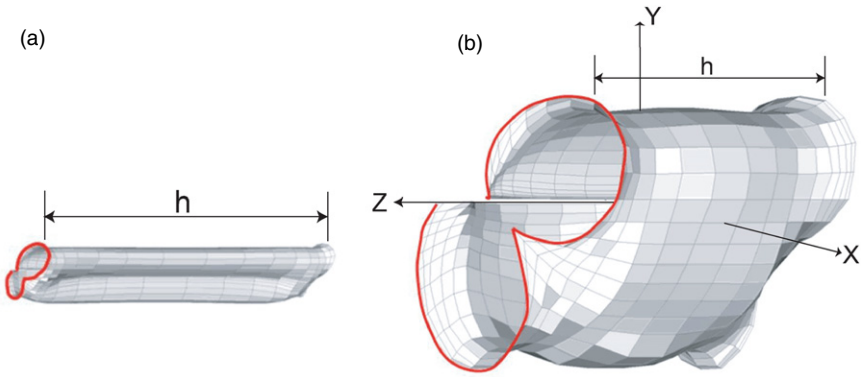

Figure 3. 3D views of the plastic zones for $M_e = 0.7$ corresponding to R_p^{max}/h of (*a*) 0.1 and (*b*) 0.5.

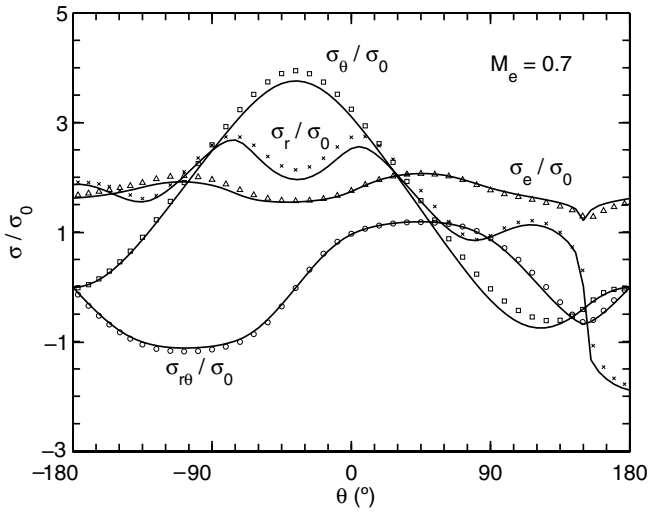

Figure 4. Comparison between 3D near-front (at r/h=0.001) angular stress distribution (symbols) corresponding to $R_p^{max}/h = 2$ at $z/h = 0.075$ and plane strain HRR solution (indicated by solid lines) for $M_e = 0.7$ (reproduced with permission [85] from [55]).

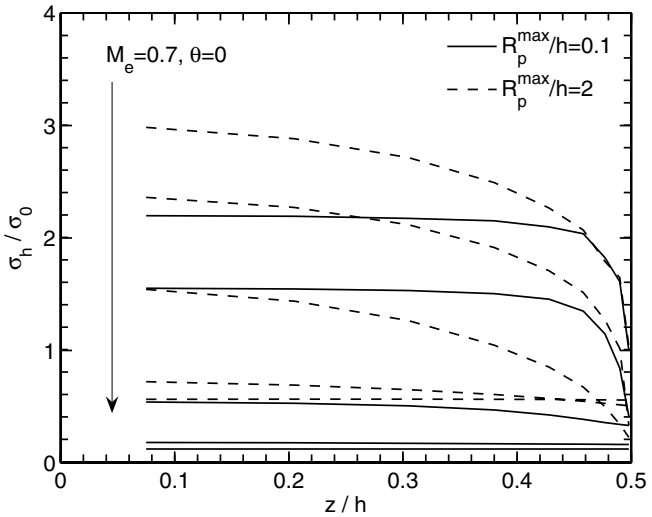

Figure 5. Variation of σ_h/σ_o with z/h at $R_p^{max}/h = 0.1$ and 2 for $M_e = 0.7$ along $\theta = 0^\circ$ (reproduced with permission [85] from [55]).The curves pertain to $r/h = 0.001$, 0.01, 0.1, 0.5 and 1.0. The arrow direction indicates increasing r/h values.

close to the crack front as will be seen later. As the load increases, transition to plane stress shape progresses towards the mid-plane of the plate. At the load level corresponding to $R_p^{max}/h = 0.5$ (figure 3(*b*)), the plastic zone at the mid-plane has almost transformed to the plane stress shape [8], whereas it still retains the plane strain characteristics near the free surface. With further increase in load, the 3D plastic zone traces all along the crack front acquire the limiting shape given by plane stress analysis. Subramanya *et al* [55] observed that for lower M_e, the transformation to plane stress shape occurs at a smaller effective stress intensity factor ($|K| = \sqrt{K_I^2 + K_{II}^2}$) as compared with that for mode I predominant loading.

Notwithstanding the shape and size of the plastic zone, Narasimhan and Rosakis [52] found that the stress distribution near the crack front in the mid-plane of a three-point bend specimen agrees closely with the plane strain HRR field. Similar agreement between the the angular stress distribution computed from 3D finite element analysis at $r/h = 0.001$ close to the mid-plane for $M_e = 0.7$ [55] and the plane strain mixed mode HRR-type solution [7] can be perceived in figure 4. This is despite the fact that figure 4 corresponds to the stage when $R_p^{max}/h = 2$ and when the plastic zone has acquired the shape given by the 2D plane stress analysis. As mentioned in section 2.1, the HRR solution indicates significantly higher stress triaxiality near the crack tip for plane strain as compared with the plane stress condition. Figure 5 shows the variations of normalized hydrostatic stress σ_h/σ_o through the plate thickness for $M_e = 0.7$ obtained by Subramanya *et al* [55]. In this figure, variations of σ_h/σ_o at different normalized radial distances r/h from the crack front for two different load levels (corresponding to $R_p^{max}/h = 0.1$ and 2) are presented. It can be seen that very near the crack front and in the interior of the plate (small r/h and z/h), where plane strain conditions apply, the hydrostatic stress is highly elevated. When the applied load is small (see solid lines in figure 5), σ_h close to the crack front ($r/h < 0.1$) is almost constant for $0 < z/h < 0.4$ and drops dramatically as the free surface is approached. At a higher load level (see dashed lines in figure 5), a more significant thickness variation of σ_h can be perceived very near the crack front. As noted in [55], this is especially true when the mode I component of loading is high as in figure 5. These results imply that vast differences in growth rates between micro-voids

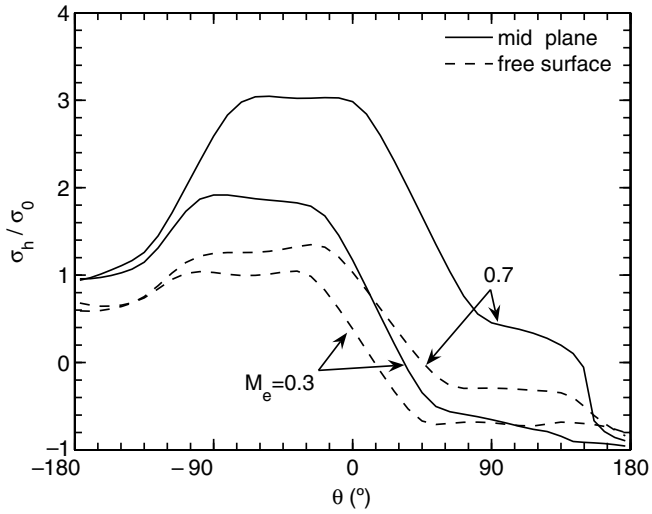

Figure 6. Angular distribution of normalized hydrostatic stress near the crack front ($r/h = 0.001$) corresponding to $R_p^{max}/h = 2$ at $z/h = 0.075$ and 0.4975 for $M_e = 0.3$ and 0.7 (reproduced with permission [85] from [55]).

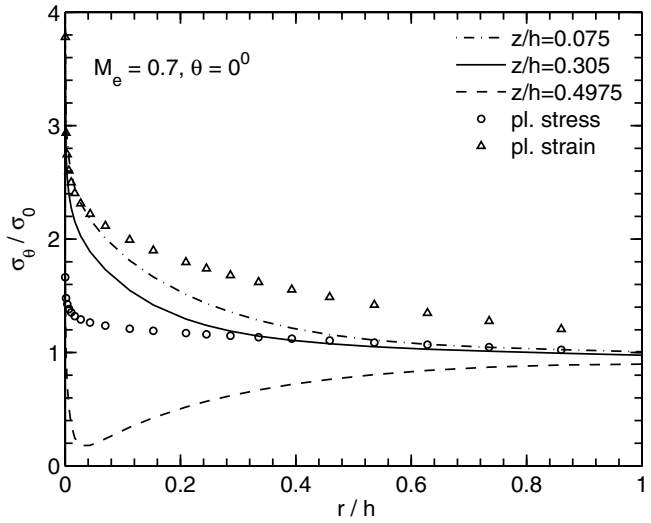

Figure 7. Radial variations of σ_θ/σ_o along three different planes normal to the crack front corresponding to $R_p^{max}/h = 2$ for $M_e = 0.7$, $\theta = 0^\circ$ (reproduced with permission [85] from [55]).

situated adjacent to the mid-plane and free surface of the plate near the crack front are expected as the load level increases. Subramanya *et al* [55] also compared these results with full-field numerical solutions based on 2D plane stress and plane strain conditions. They noted that for $r/h < 0.1$, σ_h from 3D analysis is well approximated by 2D plane strain estimates near the mid-plane. On the other hand, the stresses remain uniform through the thickness for $r/h > 0.5$, and are in reasonable agreement with the plane stress numerical solution irrespective of mode mixity and the load level.

The angular variation of the near-tip hydrostatic stress also depends on mode mixity, load level and thickness location as seen from figure 6 [55]. Here, the angular variations of σ_h/σ_o (at $r/h = 0.001$ near the mid-plane and free surface) pertaining to the stage when $R_p^{max}/h = 2$ are presented. For $M_e = 0.3$, figure 6 shows that the hydrostatic stress both near the mid-plane and the free surface attains a flat peak (or plateau) for $-90^\circ \leqslant \theta \leqslant -30^\circ$ with the mid-plane value being almost twice that at the free surface. On the other hand, for $M_e = 0.7$, this flat peak occurs in the range $-60^\circ \leqslant \theta \leqslant 0^\circ$ and its value near the mid-plane is about thrice that at the free surface. Thus, the angular location where the peak σ_h occurs shifts in the direction of negative θ as the mode II component of loading increases. Further, for a given R_p^{max}/h, the hydrostatic stress at the mid-plane is higher for mode I predominant loading. Also, for $M_e = 0.3$, σ_h is compressive both near mid-plane and at the free surface for $\theta > 30^\circ$. These observations are important since a strongly triaxial stress field influences the nucleation and growth of micro-voids, which lead to ductile fracture initiation.

Figure 7 shows the radial variation of normalized opening stress σ_θ/σ_o for $M_e = 0.7$ on three planes normal to the crack front at the load level corresponding to $R_p^{max}/h = 2$ [55]. The results obtained from 2D numerical simulations are also shown. It is seen that σ_θ determined from the plane strain simulation is higher than that computed from plane stress analysis up to a radial distance of about 0.9 h from the crack tip. The σ_θ variations determined from the 3D analyses in the interior of the plate merge with each other and with the plane strain result for small r/h. With the increase in radial distance, the stress distributions in the interior of the plate fall below the plane strain variation and approach the plane stress distribution for $r/h > 0.5$. By contrast, σ_θ near the free surface is well below the 2D plane stress curve for small r/h. It approaches the latter for $r/h > 0.8$. This was attributed by Subramanya *et al* [55] to the violation of plane stress conditions near the free surface due to the strong thickness gradient of stresses close to the crack front. However, Subramanya *et al* [55] noted that for mode II predominant loading, the radial distribution of stresses along different planes normal to the crack front approach the plane stress variation at smaller r/h (less than 0.5).

4. Numerical simulations of crack tip fields in amorphous alloys

4.1. Constitutive response of amorphous alloys

Certain metallic alloys, when subjected to high cooling rates, solidify in a disordered form leading to thin ribbons of metallic glasses or amorphous alloys [56]. Alternately, metallic glasses could be produced at relatively slow cooling rates (of the order of 1–100 K s^{-1}) in bulk form in certain multi-component alloy systems [57, 58]. These bulk metallic glasses or BMGs are believed to have many potential applications owing to their unique combination of properties such as superior tensile strength, high yield strain, reasonable fracture toughness and good corrosion resistance [59]. Although amorphous alloys are considered to be macroscopically brittle, they do exhibit substantial plastic deformation near the crack tip before fracture. However, unlike in crystalline metals, yielding in amorphous alloys is pressure/normal-stress sensitive, plastically dilatant and accompanied by strain softening [42, 60]. Furthermore, plastic flow may occur in

a heterogeneous manner by the formation of discrete shear bands [59]. Hence, classical pressure insensitive models such as the von Mises theory are inadequate to describe the mechanical response of amorphous alloys. Special constitutive theories such as the one proposed recently by Anand and Su [61] are required.

The Anand and Su model [61] is a finite strain, discrete shear-yielding, Mohr–Coulomb type theory for elastic-viscoplastic response of metallic glasses. In this model, plastic flow is assumed to occur by shearing accompanied by dilatation relative to six potential slip systems that are defined with respect to the principal directions of stress. The internal friction parameter μ is assumed to be a constant and controls the normal-stress/pressure sensitivity of yielding. The plastic dilatancy parameter χ is variable and decreases to zero with increase in plastic dilatation η. Further, plastic dilatation also controls strain softening. Thus, as η increases to a saturation level, the cohesion, c (yield strength in pure shear), monotonically decreases from its initial value c_o to a limiting value. Indeed, Anand and Su [61, 62] have demonstrated that their model can accurately represent overall features like load versus displacement response, as well as details of shear band formation during the deformation of metallic glasses in a variety of situations such as indentation and strip bending.

4.2. Mechanics of fracture of amorphous alloys

A wide range in values of the mode I fracture toughness for metallic glasses from $2\,\mathrm{MPa}\sqrt{m}$ to $80\,\mathrm{MPa}\sqrt{m}$, have been reported [63]. One of the reasons for this variability is the nature of processes occurring near the crack tip such as shear banding [64] and brittle microcracking [65]. Further, an empirical correlation between fracture toughness and Poisson's ratio of metallic glasses of different compositions has been reported in the literature [63]. The reason for this correlation from a mechanistic standpoint is not clear. Recently, the mode II fracture toughness of a Zr-based BMG was found to exceed four times its mode I fracture toughness [66], which is in contrast to that observed for crystalline alloys. Thus, many issues related to the fracture behaviour of metallic glasses are still not completely understood. These would depend strongly on the nature of the near-tip stress and deformation fields which, in turn, are influenced by the characteristic features of mechanical response of amorphous alloys such as internal friction, softening, plastic dilatation, Poisson's ratio, etc.

In order to understand the mechanics of fracture in amorphous alloys, Tandaiya *et al* [67, 68] have recently carried out detailed finite element investigations of near-tip fields around a stationary crack under mode I, plane strain, SSY conditions. The constitutive model proposed by Anand and Su [61] was employed in the simulations. The loading was applied in steps by gradually increasing the remote mode I stress intensity factor. The influence of friction parameter, flow softening and Poisson's ratio on the plastic zone, stress and deformation fields and notch opening profiles were studied. In order to gain an insight into the near-tip processes like shear banding and crack branching, plastic slipline fields and possible brittle crack trajectories around the notch root were generated. Further, the localization of plastic strain into discrete shear bands was simulated numerically by employing a statistical distribution of initial cohesion among the finite elements. Some salient results from the above studies, as well as a few very recent ones pertaining to mixed mode (I and II) loading, are presented below.

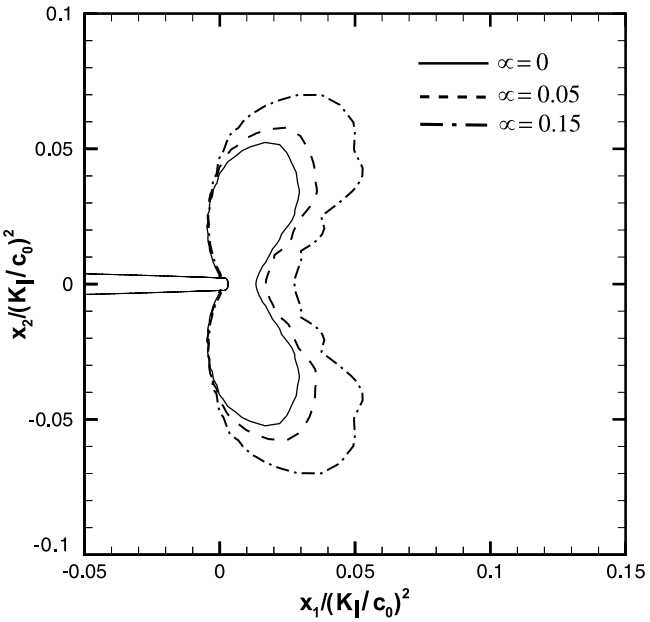

Figure 8. Effect of friction parameter μ on the normalized plastic zones in amorphous alloys corresponding to pure mode I loading (reproduced with permission [86] from [67]).

Figure 8 shows the effect of Mohr–Coulomb friction parameter μ on the plastic zones corresponding to pure mode I loading plotted in notch tip coordinates normalized by $(K_I/c_o)^2$. The plastic zone shape and size will remain invariant with respect to these normalized coordinates under SSY once the notch has blunted adequately. It can be seen from figure 8 that the plastic zone size increases with μ. In particular, the extent of the plastic zone ahead of the notch tip doubles when μ is increased from 0 to 0.15. Further, the location of the maximum extent of plastic zone rotates forward with respect to the notch line and increases from 0.05 to $0.07(K_I/c_o)^2$. The angular variation of maximum principal logarithmic plastic strain, $\ln \lambda_1^p$, around the notch tip at a normalized radius $r/(J/c_o) = 1.5$ is displayed in figure 9 corresponding to pure mode I loading condition for three different values of the friction parameter. It can be seen from figure 9 that for angles $\theta \leqslant 90^\circ$, the plastic strain level is strongly enhanced with increase in μ. Thus, the peak plastic strain increases by about 17.5% with increase in μ from 0 to 0.15 and it also occurs at smaller θ. Also, as μ increases, many distinct serrations in the near-tip angular distribution of plastic strain can be observed in the forward sector ahead of the notch tip (up to about $\theta = 90^\circ$). This corroborates with similar features perceived on the leading boundary of the plastic zone in figure 9. It suggests a tendency for plastic strains to localize into discrete shear bands, which have been observed in experiments on metallic glasses (see, for example, [64]). This

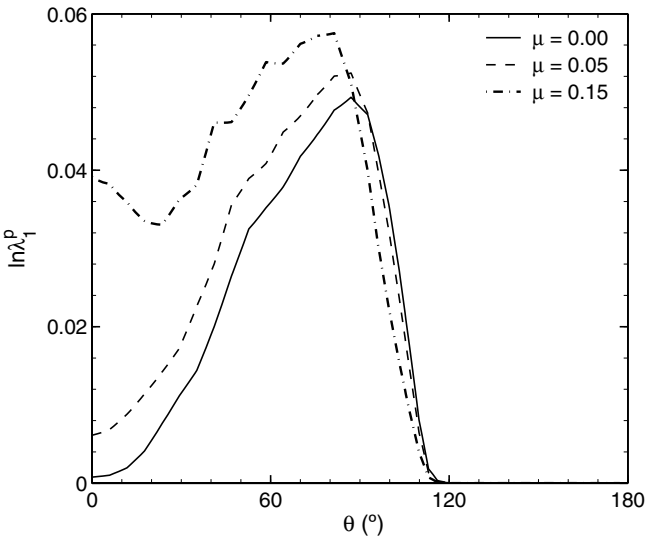

Figure 9. Effect of μ on the angular variation of maximum principal logarithmic plastic strain $\ln\lambda_1^p$ at $r/(J/c_o) = 1.5$ corresponding to pure mode I loading of amorphous alloys (reproduced with permission [86] from [67]).

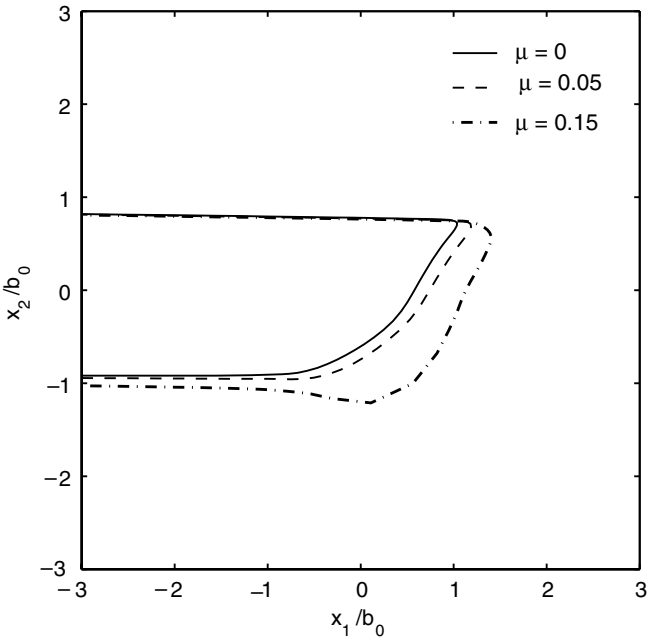

Figure 10. Effect of friction parameter μ on the deformed notch profiles in amorphous alloys corresponding to a mode II dominant mixed mode loading condition (with $M_e = 0.3$) at $|K|/(c_o\sqrt{b_o}) = 15$.

aspect is discussed later in this section.

Figure 10 shows the deformed notch profiles corresponding to $\mu = 0$, 0.05 and 0.15 under a mode II dominant mixed mode loading condition (with $M_e = 0.3$) at a normalized effective stress intensity factor of $|K|/(c_o\sqrt{b_o}) = 15$, where b_o is the initial notch root diameter. The distances are normalized by b_o. It can be seen from figure 10 that in all the three cases, the notch has deformed into a shape having a blunted lower part and a sharpened upper part. Also, an increase in μ leads to enhanced blunting and stretching of the notch surface which

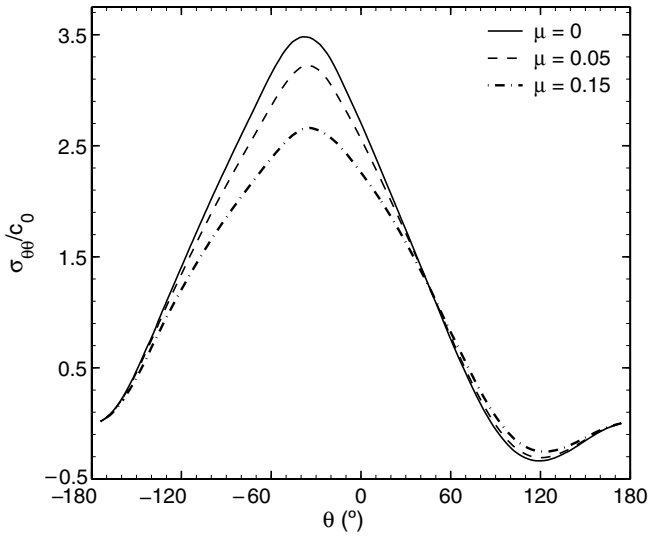

Figure 11. Effect of μ on the angular variation of tangential stress at $r/(J/c_o) = 1.5$ in amorphous alloys corresponding to a mode I dominant mixed mode loading condition (with $M_e = 0.7$).

corroborates with larger near-tip plastic strains. In figure 11, the effect of μ on the angular variation of normalized tangential stress, $\sigma_{\theta\theta}/c_o$, at a normalized radius $r/(J/c_o) = 1.5$ from the tip is presented. This figure corresponds to a mode I dominant mixed mode loading condition (with $M_e = 0.7$). It can be seen from figure 11 that the peak tangential stress occurs at $\theta = -35^\circ$ (in the blunted part of the notch) for all the three μ cases. Also, higher μ causes a dramatic decrease in the magnitude of the peak tangential stress. The effect of μ on the tangential stress is perceptible in the angular range from -120° to 50°. Further, a small compressive tangential stress can be observed for $\theta > 70^\circ$ on the upper part of the notch. In fact, the decrease in $\sigma_{\theta\theta}/c_o$ with increase in μ is found to be more pronounced for pure mode I loading as compared with mixed mode loading cases. Tandaiya *et al* [67] pointed out that the decrease in stress levels combined with enhancement in plastic strains and plastic zone size with increase in μ will suppress brittle cracking and lead to enhancement in fracture resistance. Indeed, Xi *et al* [69] have found a correlation showing direct correspondence between the fracture toughness and the plastic process zone size for various metallic glasses.

In figure 12, fringe contours of $\ln\lambda_1^p$ obtained from a simulation in which the initial value of the cohesion is varied among all elements using a normal distribution with standard deviation of 3% of the mean value c_o are presented. This figure pertains to pure mode I loading condition with $\mu = 0.15$ at a normalized load of $J/(c_o b_o) = 0.8$. It can be seen that the plastic zone contains two families of shear bands (with included angle less than 90°) that resemble discrete fingers projecting out from the notch. The intense plastic straining in a few bands close to the notch tip may cause ductile shear failure along these bands, leading to the formation of macroscopic cracks [70]. Also, it should be mentioned that the shear bands away from the notch root (not visible in figure 12) in the outer reaches of the plastic zone are similar to those observed experimentally for Vitreloy 1 metallic glass by Flores and Dauskardt [64]. It is interesting to note from figure 12 that the

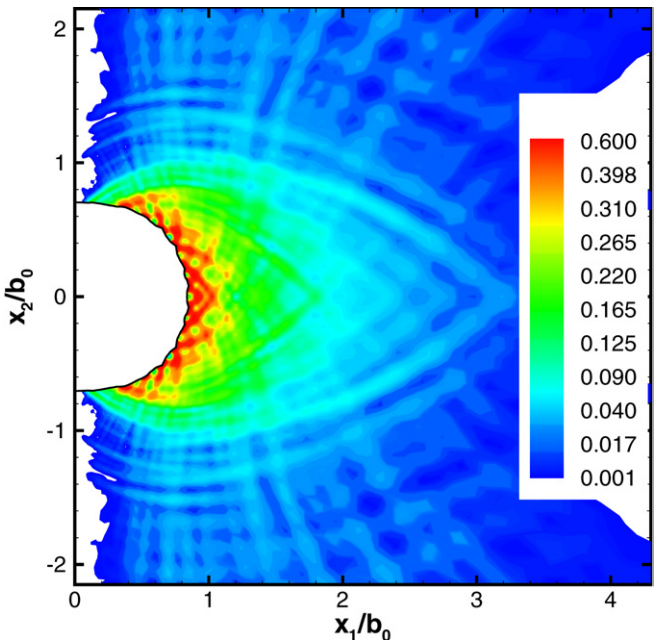

Figure 12. Contour plot of maximum principal logarithmic plastic strain $\ln \lambda_1^p$ at $J/(c_o b_o) = 0.8$ corresponding to pure mode I loading situation in amorphous alloys showing the enlarged view of the shear bands near the notch tip (reproduced with permission [86] from [67]).

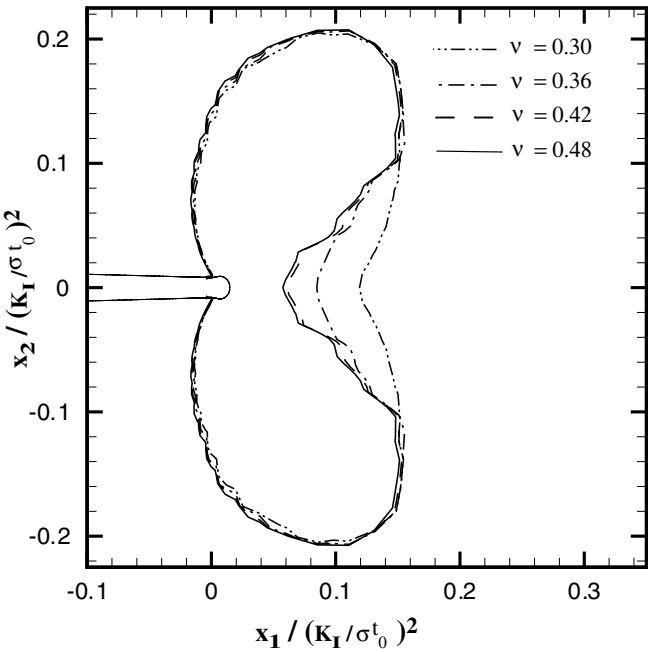

Figure 13. Effect of Poisson's ratio on the normalized plastic zone in amorphous alloys corresponding to pure mode I loading (reproduced with permission [87] from [68]).

notch surface has deformed into a shape with several vertices. These vertices form at locations on the notch surface where the two families of shear bands intersect each other and may be interpreted as shear offsets or surface steps.

The effect of varying Poisson's ratio (while keeping all other material properties the same) on the plastic zone is shown in figure 13. In this figure, the plastic zone is presented for four different values of Poisson's ratio $\nu = 0.3, 0.36, 0.42$ and 0.48. Here, notch tip coordinates are normalized by $(K_I/\sigma_o^t)^2$ where σ_o^t is the yield strength in uniaxial tension. It can be seen from figure 13 that the plastic zone size and shape are remarkably affected by the change in Poisson's ratio. Thus, with increase in ν, the plastic zone size is reduced along the leading edge, whereas it is unaffected along the trailing edge. Specifically, its extent directly in front of the notch tip is reduced by more than 50% when ν is increased from 0.3 to 0.42. Tandaiya *et al* [68] noted that this behaviour is attributed to the combined effect of normal-stress dependence of yielding, shearing accompanied by plastic dilatation and flow softening which characterize the mechanical response of BMGs. They also argued that if a ductile failure mechanism due to development of shear cracks along the shear bands is operative in the fracture process zone, then the decreased plastic strain ahead of the tip with increase in ν will delay onset of failure. This would explain, at least in part, the observed trends between fracture toughness and Poisson's ratio for metallic glasses [63].

5. Crack tip fields in ductile single crystals

In order to understand and predict the fracture behaviour of polycrystalline materials from a fundamental perspective, it is important to first investigate plastic deformation at a crack tip in a ductile single crystal. In this context, it may be noted that when the crack opening displacement is much less than the grain size, the crack tip fields are entirely contained in a single grain. Further, some key structural components are being fabricated in single crystal form. For example, blades in high pressure turbines of jet engines are made of single crystals of nickel-based superalloys.

5.1. Asymptotic analysis of crack tip fields in single crystals

Rice [71] proposed asymptotic solutions for the crack tip stress field in ductile single crystals under mode I, plane strain conditions within small strain, ideal plasticity framework. He analysed FCC and BCC crystals with the crack lying on the (0 1 0) plane and the crack front along the [1 0 $\bar{1}$] direction. The motivation for investigating this crack orientation is because it has been frequently observed to occur in experimental studies on fracture of ductile single crystals (see [72–74]). Three combinations of 3D slip systems which result in plane strain deformation were considered. For the case of the FCC single crystal, the traces of these effective slip systems are inclined at 55°, 125° and 0° to the crack line in the plane of deformation (the x_1–x_2 plane). The Schmid law was considered as the anisotropic yield criterion, which for the 2D effective slip systems leads to a hexagonal yield locus in the stress plane with axes given by $(\sigma_{11} - \sigma_{22})/2\tau_o$ and σ_{12}/τ_o, where τ_o is the critical resolved shear stress. Rice [71] assumed that for a stationary crack the yield condition can be met asymptotically all around the crack tip, thus requiring discontinuities in the stress state to satisfy the equilibrium condition. His solution consists of four constant stress sectors separated by stress and displacement discontinuities. The Cartesian stress components prevailing in

Table 1. Cartesian stress components prevailing in different slip sectors in the asymptotic near-tip solution of Rice [71] for ideally plastic FCC single crystal.

Sector	Angular range	σ_{22}/τ_o	σ_{11}/τ_o	σ_{12}/τ_o
A	0°–54.74°	7.35	4.9	0
B	54.74°–90°	4.9	3.67	−1.73
C	90°–125.26°	2.45	3.67	−1.73
D	125.26°–180°	0	2.45	0

the four constant stress sectors, labelled A, B, C and D, in the case of the FCC single crystal are summarized in table 1. It must be noted that the stress triaxiality in the region ahead of the tip is very high ($\sigma_h/\tau_o = 5.3$) and hence this solution should apply to high constraint geometries such as deeply cracked three-point bend specimen. Rice [71] also predicted intense shear, either in slip mode or kink mode, along the sector boundaries. Thus, corresponding to the FCC crystal, Rice's solution involves slip shear bands at $\theta = 55°$ and 125° and kink shear band at 90°.

Saeedvafa and Rice [75] obtained HRR-type asymptotic solutions for crack tip fields in power law hardening single crystals. They assumed a simple Taylor (isotropic) hardening model. In the limit of small hardening, their angular stress distribution converges to the solution of Rice [71]. Drugan [76] extended Rice's analysis to derive asymptotic solutions without kink-sector boundary by introducing sub-yield near-tip sector and applying full stress continuity at the elastic–plastic sector boundaries. He showed that the presence of such an elastic sector can lower the stress triaxiality ahead of the crack tip.

5.2. Numerical simulations of mechanics of fracture of single crystals

Cuitino and Ortiz [77] numerically studied three-dimensional crack tip fields in copper single crystals loaded in a four-point bending configuration. Their calculations were based on a dislocation hardening model and showed notable differences in the slip activity at the free surface and in the interior of the specimen. Flouriot *et al* [78] carried out three-dimensional finite element simulations of a compact tension specimen to investigate the mode I crack tip fields in elastic-perfectly plastic FCC single crystals of Ni-based superalloys. They demonstrated the highly three-dimensional nature of plastic strain fields and compared their numerical results against experimental data. Patil *et al* [79] performed a combined numerical and experimental study of crack tip fields in a single edge notched (tensile) specimen (SENT) of an aluminium single crystal. The analysis was conducted from contained to large scale yielding conditions. They considered the crack orientation analysed by Rice [71], but found much less triaxiality and also a different near-tip distribution of plastic slip in the above specimen as compared with that expected on the basis of Rice's solution. In particular, they noted that two kink shear bands (involving lattice rotation) may form at $\theta = 90°$ and about $\theta = 45°$ with respect to the notch line which was confirmed from observations using electron back scattered diffraction (EBSD) on the specimen surface. These discrepancies suggested possible strong configuration dependence of the near-tip fields in ductile single crystals under large scale yielding conditions, which was actually predicted by Rice [71].

In order to understand the above issue, Patil *et al* [80] recently studied the effect of crack tip constraint on stress and plastic strain distributions in FCC single crystal, having the orientation considered by Rice [71], under mode I, plane strain conditions. They performed finite element simulations by employing a two-parameter (stress intensity factor K and T-stress) based modified boundary layer approach within crystal plasticity framework (ignoring elastic anisotropy). They generated solutions corresponding to different values of T/τ_o, which indicates the level of crack tip constraint, with $T/\tau_o \geqslant 0$ representing high constraint while $T/\tau_o < 0$ signifies low constraint. The fringe contours of the maximum principal logarithmic plastic strain, $\ln(\lambda_1^p)$, obtained by Patil *et al* [80] for $T/\tau_o = 0$ and -2 at $K/(\tau_o\sqrt{b_o}) = 80$ are displayed in figures 14(*a*) and (*b*), respectively. It can be observed from these figures that the T-stress has a significant effect on the plastic zone shape and size, which is akin to isotropic plastic solids. The shape of the plastic zone is governed by the shear bands that form due to plastic slip on various systems. For $T/\tau_o = 0$, distinct contributions from two slip shear bands at angles of about 55° and 125° to the notch line, and a kink shear band at an angle of 90° (as predicted by Rice [71]) to the plastic zone shape can be perceived in figure 14(*a*). By contrast, the predominant contribution to the plastic strain distribution for $T/\tau_o < 0$ (see, figure 14(*b*)) comes from the slip shear band inclined at an angle of 55° to the notch line.

The near-tip stress distribution is significantly affected by the constraint level. The radial variations of the normalized opening stress (σ_{22}/τ_0) with normalized distance $r/(J/\tau_o)$ ahead of the notch tip as given by Patil *et al* [80] are displayed in figure 15, corresponding to different levels of constraint. It can be noted from the figure that negative T causes a significant downward shift in the radial variation of σ_{22}, while positive T tends to marginally increase the opening stress above the $T = 0$ case. It is also evident from figure 15 that the curves pertaining to different values of T/τ_o are roughly parallel to each other for $r/(J/\tau_0) > 2$. This suggests that the deviation of σ_{22} from the $T = 0$ case is essentially independent of normalized distance, $r/(J/\tau_o)$, from the notch tip.

Figure 16 shows the trajectories of the stress state encountered on traversing around the notch tip from $\theta = 0$ (line ahead of the notch tip) to $\theta \to \pi$ (notch flank) in the stress plane. Results extracted at a normalized radial distance of $r/(J/\tau_o) = 4$ from the notch tip are presented corresponding to $T/\tau_o = 1, 0, -0.5, -0.85$ and -1.5. It can be observed that for $T/\tau_o > 0$ the trajectory in the stress plane follows the yield locus ABCD, which is similar to that given by the asymptotic solution of Rice [71]. Thus, the stress state all around the crack tip is at yield for $T/\tau_o > 0$. However, as T/τ_0 decreases, the stress state initially follows the yield locus but later deviates and falls inside it which implies the presence of an elastic sector in the near-tip region. As already mentioned, Drugan [76] showed that the presence of an elastic sector near the crack tip may reduce the stress triaxiality. On imposition of further negative T-stress, a plastic

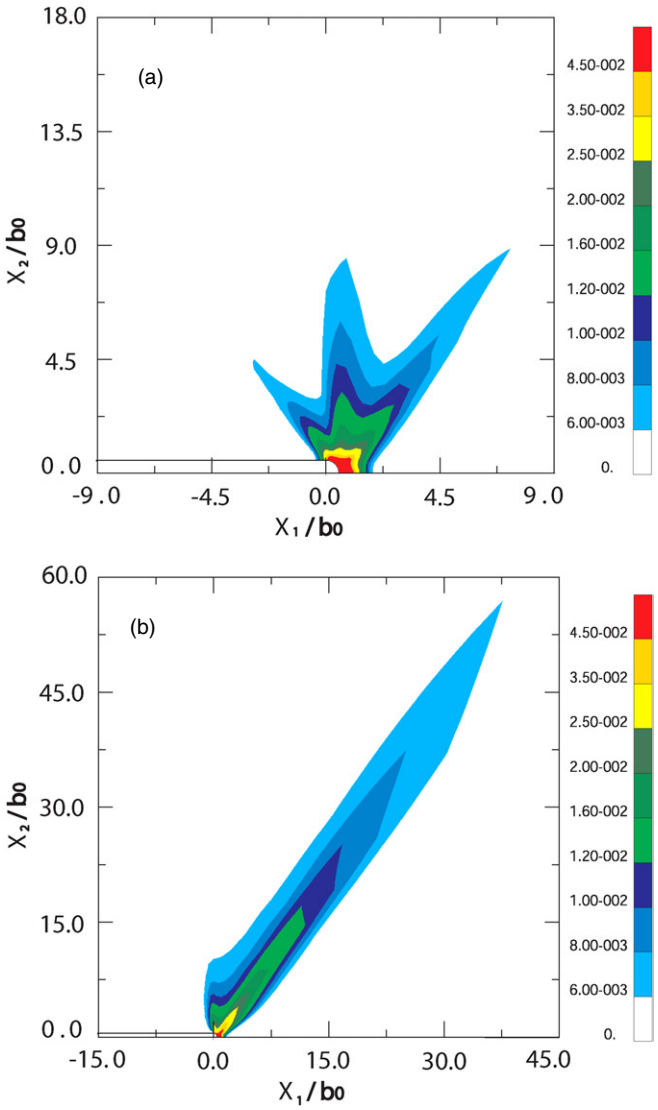

Figure 14. Fringe contour plots of maximum principal logarithmic plastic strain $\ln \lambda_1^p$ in FCC single crystal corresponding to (*a*) $T = 0$ and (*b*) $T = -2\tau_o$ and the same level of $K/(\tau_o\sqrt{b_o}) = 80$ (reproduced with permission [88] from [80]).

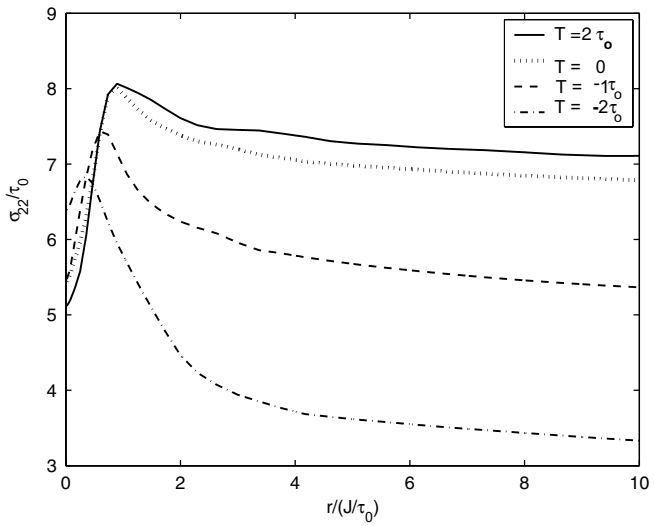

Figure 15. Radial variations of opening stress (σ_{22}/τ_0) at $\theta = 0^\circ$ in FCC single crystals, for $T/\tau_0 = 2, 0, -1$ and -2 and the same level of $K/(\tau_o\sqrt{b_o}) = 80$ (reproduced with permission [88] from [80]).

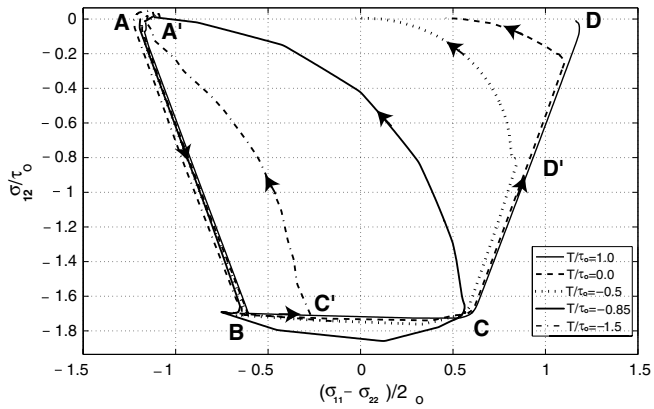

Figure 16. Trajectories plotted in the stress plane of the state encountered on traversing around the crack tip at $r/(J/\tau_o) = 4$ in FCC single crystal obtained from finite element analysis with different T/τ_o values.

sector develops adjacent to the notch flank and the stress state prevailing in this plastic sector corresponds to vertex A. Moreover, the point at which elastic unloading starts shifts from vertex D and progressively approaches first vertex C and then vertex B as T/τ_o changes from a high positive to a high negative value. It is important to emphasize that the trajectories presented in figure 16 are different from those proposed by Drugan [76]. In his asymptotic solution, the stress state in the elastic sector is taken to vary along an arc commencing from point B and ending at point D in figure 16. In other words, it was assumed by Drugan [76] that the plastic sector at the crack surface corresponds to vertex D, instead of vertex A as suggested by figure 16.

In figure 17, angular variations of effective plastic slip, γ, for all three conjugate slip system pairs at $r/(J/\tau_o) = 4$ reported by Patil *et al* [80], corresponding to $T/\tau_o = 2, 0, -1$ and -2 are presented. Figure 17(*a*) shows that plastic slip on the pair of conjugate systems $(1\,\bar{1}\,1)[1\,1\,0]$ and $(1\,\bar{1}\,1)[0\,1\,1]$ attains a peak value at about $\theta \approx 55^\circ$, irrespective of the level of T-stress. Thus, the slip activity on this pair of systems results in a slip shear band. It can be observed from figure 17(*a*) that the peak value of γ enhances strongly with increase in T-stress in the negative direction. The effective plastic slip on conjugate pair $(1\,1\,1)[1\,\bar{1}\,0]$ and $(1\,1\,1)[0\,1\,\bar{1}]$ (figure 17(*b*)) shows a more interesting response to different T-stress levels. For high positive T, the peak value of slip in this system occurs at about $\theta = 125^\circ$ and hence leads to the development of a dominant slip shear band at this angle. On the other hand, for high negative T, the peak value is observed at $\theta = 35^\circ$ to 45°, resulting in the development of a kink shear band at this angle to the notch line. The slip activity on the pair of systems $(\bar{1}\,1\,1)[1\,0\,1]$ and $(1\,1\,\bar{1})[1\,0\,1]$, displayed in figure 17(*c*), shows the peak occurring at about $\theta \approx 90^\circ$, irrespective of T-stress level and leads to a kink shear band at this angle. This corroborates the recent EBSD results obtained by Patil *et al* [81] on a high constraint three-point bend specimen of an aluminium single crystal which has clearly shown the existence of lattice misorientation bands at $\pm 90^\circ$ to

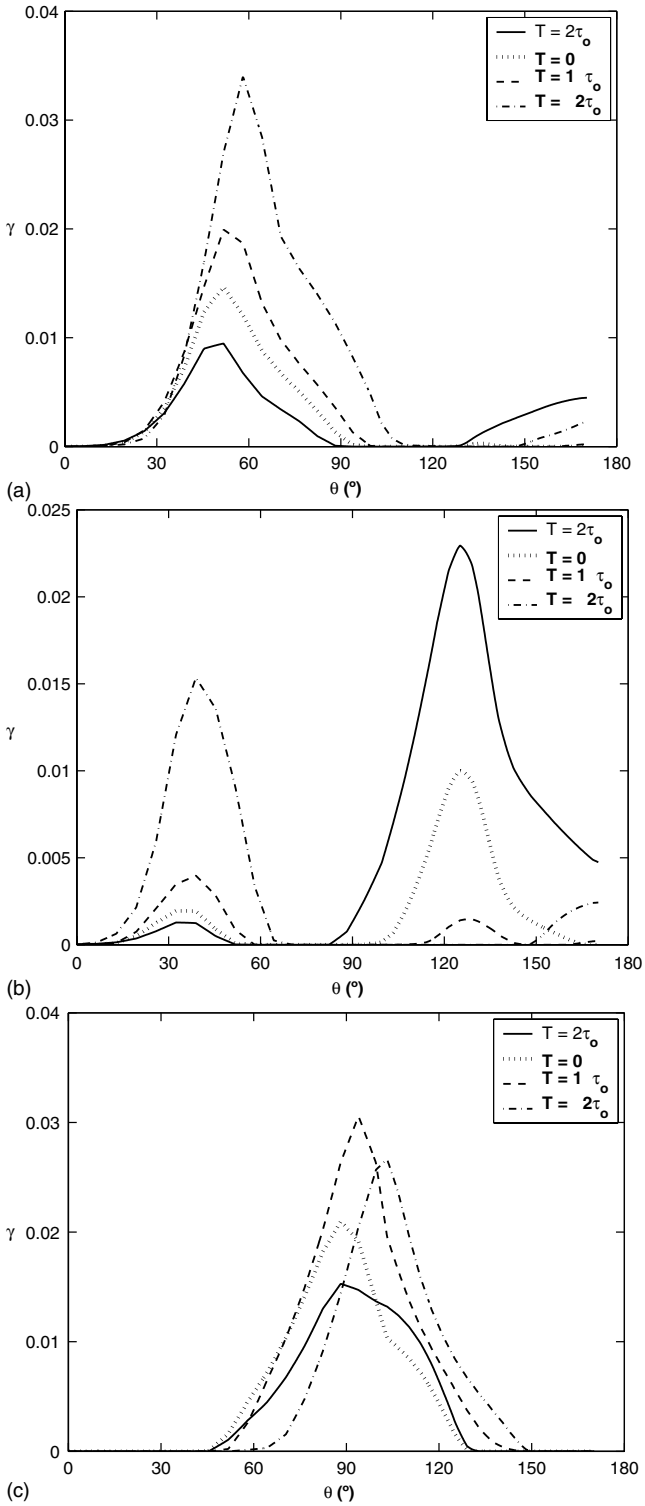

Figure 17. Angular variations of effective plastic slip γ on all three conjugate slip system pairs in FCC single crystal: (*a*) $(1\,\bar{1}\,1)[1\,1\,0]$ and $(1\,\bar{1}\,1)[0\,1\,1]$, (*b*) $(1\,1\,1)[1\,\bar{1}\,0]$ and $(1\,1\,1)[0\,1\,\bar{1}]$ and (*c*) $(\bar{1}\,1\,1)[1\,0\,1]$ and $(1\,1\,\bar{1})[1\,0\,1]$ at $r/(J/\tau_0) = 4$ for $T/\tau_0 = 2, 0, -1$ and -2 and same level of $K/(\tau_o\sqrt{b_o}) = 80$ (reproduced with permission [88] from [80]).

the notch line. Furthermore, as already mentioned, Patil *et al* [79] have reported that two kink shear bands (involving lattice rotation) form at $\theta = 90^\circ$ and about $\theta = 45^\circ$ with respect to the notch line in a low constraint SENT specimen.

Thus, the work of Patil *et al* [79–81] has shown that the stress distribution near a crack tip in a ductile single crystal will depend strongly on the constraint level with elastic sectors present in low constraint geometries. Furthermore, the slip activity in ductile single crystals is also profoundly influenced by crack tip constraint resulting in possible fascinating dependence of slip and kink shear band patterns near a crack tip on the fracture configuration.

6. Concluding remarks

In this review, various facets associated with recent simulations of 3D mixed mode elastic–plastic fields near a crack front, mechanics of fracture of amorphous alloys and constraint effects in single crystals, have been briefly highlighted. These illustrate that numerical simulations aimed at delineating crack tip fields have made considerable progress, particularly because of the availability of powerful computational resources as well as continuous development of efficient algorithms. Further, formulation of increasingly precise constitutive laws for describing the response of both conventional as well as new materials also enables detailed assessment of their fracture behaviour. Due to these advances, it is now possible to apply fracture mechanics concepts in a variety of situations of engineering importance. Nevertheless, considerable amount of work still needs to be performed. These include characterization of crack tip fields in cellular materials, wherein the characteristic microstructural length scale is in millimetres, and shape memory alloys, where, in addition to plasticity, transformation induced strains can also accrue ahead of a crack tip [82]. Furthermore, polycrystal plasticity simulations [83] of crack tip fields are important because they can account for evolution of texture near the tip and also incorporate effects such as dislocation based hardening mechanisms and grain size. These effects cannot be captured using phenomenological anisotropic plasticity theories such as that due to Hill [29].

It must be emphasized that simulations cannot predict the fracture resistance of a given material *per se* unless failure criteria based on physical mechanisms are explicitly introduced into the simulations (see, for example, [26, 84]). The latter make detailed experimental characterization indispensable. Indeed, advances in experimental methods such as crack tip strain field mapping using digital image correlation (DIC), optical methods such as interferometry and caustics, tomography using synchrotron radiation and microscopy techniques such as EBSD have made such characterization possible [53, 82, 81]. Simultaneously, efforts are being made to link the continuum descriptions of a solid with atomistic aspects through molecular dynamics and discrete dislocation plasticity simulations. However, bridging the length scales in a seamless fashion and yet without the loss of fidelity of the simulations remains a challenge to be addressed.

Acknowledgments

Parag Tandaiya would like to thank the John Argyris Foundation for granting an Argyris Scholarship in Computational Mechanics at the Indian Institute of Science, Bangalore.

References

[1] Hutchinson J W 1968 *J. Mech. Phys. Solids* **16** 13–31
[2] Hutchinson J W 1968 *J. Mech. Phys. Solids* **16** 337–42
[3] Rice J R and Rosengren G F 1968 *J. Mech. Phys. Solids* **16** 1–12
[4] Rice J R 1968 *ASME J. Appl. Mech.* **35** 379–86
[5] Symington M, Ortiz M and Shih C F 1990 *Int. J. Fract.* **45** 51–64
[6] Hutchinson J W 1983 *ASME J. Appl. Mech.* **50** 1042–51
[7] Shih C F 1974 Small-scale yielding analysis of mixed-mode plane-strain crack problems *Fracture Analysis* (Philadelphia, PA: ASTM STP) vol 560 pp 187–210
[8] Hutchinson J W and Shih C F 1975 Plastic analysis of mixed mode plane stress crack problems *Recent Advances in Engineering Science* ed T S Chang (Boston: Scientific Publishers) pp 245–53
[9] Pan J and Shih C F 1990 *J. Mech. Phys. Solids* **38** 161–81
[10] Pan J and Shih C F 1990 *J. Appl. Mech.* **57** 259–67
[11] Pan J and Shih C F 1992 *Int. J. Solids Struct.* **29** 2795–814
[12] Shih C F and Asaro R J 1988 *J. Appl. Mech.* **55** 219–316
[13] Shih C F and Asaro R J 1989 *J. Appl. Mech.* **56** 577–84
[14] Shih C F and Asaro R J 1991 *J. Appl. Mech.* **58** 450–63
[15] Shih C F 1991 *Matl. Sci. Eng.* A **143** 77–90
[16] McMeeking R M and Parks D M 1979 On the criteria for *J* dominance of crack tip fields in large scale yielding *Elastic–Plastic Fracture Mechanics* (ASTM STP) vol 668 pp 175–94
[17] Shih C F and German M D 1981 *Int. J. Fract.* **17** 27–43
[18] McClintock F A 1971 Plasticity aspects of fracture *Fracture: An Advanced Treatise* ed H Liebowitz (New York: Academic Press) pp 47–225
[19] Sharma S M and Aravas N A 1991 *J. Mech. Phys. Solids* **39** 1043–72
[20] Xia L, Wang T C and Shih C F 1993 *J. Mech. Phys. Solids* **41** 665–87
[21] Betegon C and Hancock J W 1991 *J. Appl. Mech.* **58** 104–10
[22] O'Dowd N P and Shih C F 1991 *J. Mech. Phys. Solids* **39** 989–1015
[23] Arun Roy Y and Narasimhan R 1997 *Int. J. Fract.* **88** 259–79
[24] Basu S and Narasimhan R 2000 *J. Mech. Phys. Solids* **48** 1967–85
[25] Jayadevan K R, Narasimhan R, Ramamurthy T S and Dattaguru B 2002 *Int. J. Fract.* **116** 141–60
[26] Biswas P and Narasimhan R 2002 *Mech. Mater.* **34** 577–92
[27] Pan J and Shih C F 1986 *Mech. Mater.* **5** 299–316
[28] Pan J and Shih C F 1988 *Int. J. Fract.* **37** 171–95
[29] Hill R 1950 *The Mathematical Theory of Plasticity* (Oxford: Clarendon Press)
[30] Stelmashenso M A, Walls M G, Brown L M and Miman Y V 1993 *Acta Met. Mater.* **41** 2855–65
[31] Fleck N A, Muller G M, Ashby M F and Hutchinson J W 1994 *Acta Met. Mater.* **42** 475–87
[32] Stolken J S and Evans A G 1998 *Acta Mater.* **46** 5109–15
[33] Fleck N A and Hutchinson J W 1994 *J. Mech. Phys. Solids* **41** 1825–57
[34] Fleck N A and Hutchinson J W 1997 Strain gradient plasticity *Advances in Applied Mechanics* vol 33, ed J W Hutchinson and T T Wu pp 295–361
[35] Gao H, Huang Y, Nix W D and Hutchinson J W 1999 *J. Mech. Phys. Solids* **47** 1239–63
[36] Elssner G, Korn D and Ruehle M 1994 *Scr. Met. Mater.* **31** 1037–42
[37] Xia Z C and Hutchinson J W 1996 *J. Mech. Phys. Solids* **44** 1621–48
[38] Huang Y, Zhang L, Guo T F and Hwang K C 1997 *J. Mech. Phys. Solids* **45** 439–65
[39] Jiang H, Huang Y, Zhuang Z and Hwang K C 2001 *J. Mech. Phys. Solids* **49** 979–93
[40] Spitzig W A and Richmond O 1979 *Polym. Eng. Sci.* **19** 1129–39
[41] Chen I-W and Reyes-Morel P E 1986 *J. Am. Ceram. Soc.* **69** 181–9
[42] Lu J and Ravichandran G 2003 *J. Mater. Res.* **18** 2039–49
[43] Bardia P and Narasimhan R 2006 *Strain* **42** 187–97
[44] Rudnicki J W and Rice J R 1975 *J. Mech. Phys. Solids* **23** 371–94
[45] Li F Z and Pan J 1990 *Trans. ASME: J. Appl. Mech.* **57** 40–9
[46] Li F Z and Pan J 1990 *Eng. Fract. Mech.* **35** 1105–16
[47] Subramanya H Y, Viswanath S and Narasimhan R 2008 *Eng. Fract. Mech.* **75** 1045–63
[48] Yuan H and Lin G 1993 *Int. J. Fract.* **61** 295–330
[49] Chiang M Y M and Chai H 1994 *Int. J. Solids Struct.* **31** 2477–90
[50] Papanastasiou P and Durban D 2001 *Int. J. Solids Struct.* **38** 1539–50
[51] Nakamura T and Parks D M 1990 *J. Mech. Phys. Solids* **38** 787–812
[52] Narasimhan R and Rosakis A J 1990 *Trans. ASME: J. Appl. Mech.* **57** 607–17
[53] Zehnder A T and Rosakis A J 1990 *Trans. ASME: J. Appl. Mech.* **57** 618–26
[54] Subramanya H Y, Viswanath S and Narasimhan R 2007 *Int. J. Solids Struct.* **44** 1863–79
[55] Subramanya H Y, Vishwanath S and Narasimhan R 2005 *Int. J. Fract.* **136** 167–85
[56] Klement W, Willens R H and Duvez P 1960 *Nature* **187** 869–70
[57] Inoue A 2000 *Acta Mater.* **48** 279–306
[58] Johnson W L 1999 *MRS Bull.* **24** 7249–51
[59] Schuh C A, Hufnagel T C and Ramamurty U 2007 *Acta Mater.* **55** 4067–109
[60] Bhowmick R, Raghavan R, Chattopadhyay K and Ramamurty U 2006 *Acta Mater.* **54** 4221–8
[61] Anand L and Su C 2005 *J. Mech. Phys. Solids* **53** 1362–96
[62] Anand L and Su C 2006 *Acta Mater.* **54** 179–89
[63] Lewandowski J J, Wang W H and Greer A L 2005 *Phil. Mag. Lett.* **85** 77–87
[64] Flores K M and Dauskardt R H 1999 *Scr. Mater.* **41** 937–43
[65] Lowhaphandu P and Lewandowski J J 1998 *Scr. Mater.* **38** 1811–17
[66] Flores K M and Dauskardt R H 2006 *J. Mech. Phys. Solids* **54** 2418–35
[67] Tandaiya P, Narasimhan R and Ramamurty U 2007 *Acta Mater.* **55** 6541–52
[68] Tandaiya P, Ramamurty U, Ravichandran G and Narasimhan R 2008 *Acta Mater.* **56** 6077–86
[69] Xi X K, Zhao D Q, Pan M X, Wang W H, Wu Y and Lewandowski J J 2005 *Phys. Rev. Lett.* **94** 125510
[70] Conner R D, Johnson W L, Paton N E and Nix W D 2003 *J. Appl. Phys.* **94** 904–11
[71] Rice J R 1987 *Mech. Mater.* **6** 317–35
[72] Neumann P 1974 *Acta Metall.* **22** 1155–65
[73] Neumann P 1974 *Acta Metall.* **22** 1167–78
[74] Garrett G and Knott J 1975 *Acta Metall.* **23** 841–8
[75] Saeedvafa M and Rice J R 1989 *J. Mech. Phys. Solids* **37** 673–91
[76] Drugan W J 2001 *J. Mech. Phys. Solids* **49** 2155–76
[77] Cuitino A M and Ortiz M 1996 *J. Mech. Phys. Solids* **44** 863–99
[78] Flouriot S, Forest S, Cailletaud G, Koster A, Remy L, Burgardt B, Gros V, Mosset S and Delautre J 2003 *Int. J. Fract.* **124** 43–77
[79] Patil S D, Narasimhan R, Biswas P and Mishra R K 2008 *ASME J. Eng. Mater. Technol.* **130** 1–11

[80] Patil S D, Narasimhan R and Mishra R K 2008 *J. Mech. Phys. Solids* **56** 2265–86
[81] Patil S D, Narasimhan R and Mishra R K 2009 Observation of kink shear bands in an aluminium single crystal fracture specimen, submitted
[82] Daly S, Bhattacharya K and Ravichandran G 2008 Deformation and fracture behavior of a shape memory alloy, NITINOL. *Proc. of the Interquadrennial Conf. of the Int. Congress on Fracture (Bangalore)* ed B K Raghu Prasad and R Narasimhan (New Delhi: I. K. International Publishing House Pvt. Ltd) pp 10–12
[83] Kalidindi S R, Bronkhorst C A and Anand L 1992 *J. Mech. Phys. Solids* **40** 536–69
[84] Chew H B, Guo T F and Cheng L 2007 *Int. J. Solids Struct.* **44** 2553–70
[85] With kind permission from Springer Science+Business Media: Subramanya H Y, Vishwanath S and Narasimhan R 2005 A three-dimensional numerical study of mixed mode (I and II) crack tip fields in elastic–plastic solids *Int. J. Fract.* **136** 167 (figures 1(a), 4, 5, 7, and 12(b), and any original (first) copyright notice displayed with material)
[86] Reprinted from Tandaiya P, Narasimhan R and Ramamurty U 2007 Mode I crack tip fields in amorphous materials with application to metallic glasses *Acta Mater.* **55** 6541–52 (with permission from Elsevier)
[87] Reprinted from Tandaiya P, Narasimhan R and Ramamurty U 2008 Effect of Poisson's ratio on crack tip fields and fracture behavior of metallic glasses *Acta Mater.* **56** 6077–86 (with permission from Elsevier)
[88] Reprinted from Patil S D, Narasimhan R and Mishra R K 2008 A numerical study of crack tip constraint in ductile single crystals *J. Mech. Phys. Solids* **56** 2265–86 (with permission from Elsevier)